

Design of IRS-Assisted Non-Binary Channel-Coded Physical Layer Network Coding

Mahmoud AlaaEldin*, Emad Alsusa*, and Karim G. Seddik†

*Electrical and Electronic Engineering Department, University of Manchester, Manchester, UK M13 9PL

†Department of Electronics and Communications Engineering, American University in Cairo, Cairo, Egypt 11835
mahmoud.alaeldin@manchester.ac.uk, e.alsusa@manchester.ac.uk, kseddik@aucegypt.edu

Abstract—In this paper, we present an intelligent reflective surface (IRS)-assisted physical layer network coding (PNC) system in a two-way relaying channel (TWRC). Specifically, IRS is used to align the effective channels of the two received superimposed signals at the relay, which allows canceling the carrier phase offset (CPO) between the two received signals. The IRS phase shifts are optimized to maximize the received PNC signal amplitude while having a zero CPO constraint. An efficient manifold optimization-based approach is proposed to solve this problem, where the optimization is performed on the complex circle manifold. Moreover, we improve the performance of channel-coded IRS-assisted PNC by introducing the weighted non-binary PNC (WN-PNC) scheme, where the binary data are mapped to, and encoded over, Galois Fields (GFs). We present two WN-PNC cases where the data is encoded over GF(4) and GF(8), then modulated using quadrature phase shift keying (QPSK) and 8-quadrature amplitude modulation (8-QAM), respectively. We also design proper PNC mapping functions for both cases, ensuring that no PNC ambiguity can occur at the relay. Our simulation results show the efficacy of the proposed manifold optimization-based approach and the error performance improvement of the WN-PNC over the binary PNC case.

I. INTRODUCTION

The research on physical layer network coding (PNC) has attracted much attention in the wireless communication society during the last two decades. This is because PNC can scale up the network's throughput, especially when multiple nodes share information through intermediate relays [1]. On another note, the intelligent reflective surfaces (IRS) technology have been introduced in literature during the past few years, and it has been shown to improve the performance of wireless systems by controlling the wireless channel [2], [3]. In this paper, we study the integration of IRS into a PNC system in a two-way relaying channel (TWRC).

IRS has risen during the past few years as a prominent technology for wireless systems [2]–[4]. An IRS panel is a surface that has a large number of radio frequency (RF) passive reflecting elements which can engineer the wireless channel. The IRS reflecting elements can control the amplitudes and phases of the incident signals before reflection to achieve various design aims for wireless systems, like interference suppression and signal strengthening. Therefore, IRS can be regarded as a promising solution to improve the spectral and energy efficiency of the wireless systems [5]. Hence, many works in the literature have investigated the application of IRS in many wireless communication systems. For example,

the application of IRS has been studied in the context of multi-user wireless systems [6]–[9], non-orthogonal multiple access (NOMA) networks [10]–[12], wireless information and power transfer [13], [14], unmanned aerial vehicles (UAV) communications [15], and physical layer security [16].

On the other hand, in the PNC literature, many works have investigated and provided practical solutions to the carrier phase offset (CPO) problem in the TWRC. The CPO problem is defined as the phase difference between the two superimposed received signals at the relay in the TWRC due to having different fading channels from the two end nodes to the relay. The CPO problem becomes even more challenging in the context of channel-coded PNC, where the two end nodes want to exchange channel-coded information through the relay. In this case, the relay has to decode network-coded information from the received superimposed codewords while dealing with the CPO. In [17], the CPO problem was studied for a channel coded PNC in a TWRC, where the authors proposed a solution to the CPO utilizing the symbols misalignment between the two signals when decoding the network coded information. In [18], a linear modulation and coding scheme was proposed where linear combinations of the information symbols are computed at the relay. The network coding coefficients were chosen to approximate the fading coefficients of the channels. The authors in [19] proposed a solution for the CPO in a heterogeneous PNC scheme in a TWRC using an adaptive mapping function at the relay. The mapping function adapts according to the relative difference between the two fading channels in the TWRC. The authors extended their design in [20] to include channel coding in the heterogeneous PNC. In [21], the authors utilized the difference between the channel coefficients to adapt the PNC mapping function to decrease the impact of the interference at the relay. In [22], the performance of asynchronous PNC was analyzed by deriving the symbol error rate (SER) of the system, taking into account both phase and symbol mismatch. In [23], the authors considered the use of binary frequency shift keying (BFSK) to reduce the effect of the CPO.

In this paper, a simple design for an IRS-assisted PNC in a TWRC is presented. More specifically, the IRS phase shifts are optimized to cancel the CPO between the two superimposed signals at the relay while maximizing the amplitude of the received signals. This adjustment allows the IRS to align the two received signals at the relay, simplifying the PNC

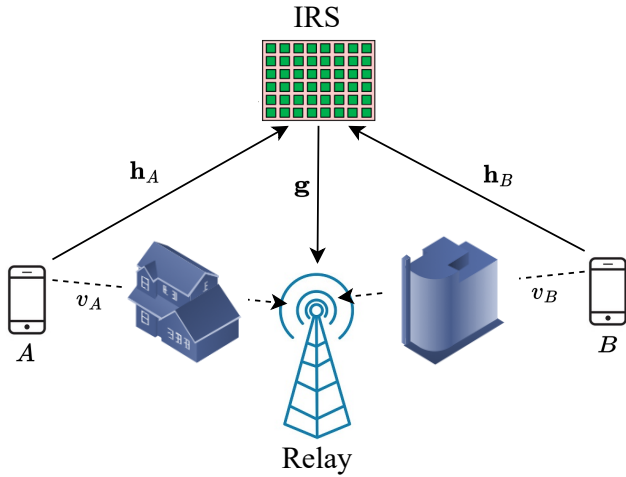


Figure 1: IRS aided PNC in TWRC

mapping function design at the relay. The PNC mapping function maps the superimposed signal to a network-coded signal. To that end, an efficient manifold optimization-based algorithm is proposed to find a solution for the IRS phase shifts that solves the proposed PNC optimization problem. Moreover, we design a repeat accumulate (RA) channel coded IRS-assisted PNC and further enhance its performance by introducing the weighted non-binary PNC (WN-PNC) scheme. The WN-PNC is designed for the cases of quadrature phase shift keying (QPSK) and 8-quadrature amplitude modulation (8-QAM) modulation schemes, whereas the data is encoded over the Galois field (GF) of sizes 4 and 8, respectively. The WN-PNC mapping function for both cases is designed so that no mapping ambiguity can occur at the relay. This work differs from our previous work in [24] where we have considered channel coded PNC over the Ring to extend to higher modulation orders. However, in this paper, we propose the WN-PNC considering QPSK and 8-QAM, and our results show that the proposed WN-PNC provides enhanced performance when compared against the binary case with comparable decoding complexities.

II. SYSTEM MODEL

We present an IRS-assisted PNC system in a TWRC as a means of exchanging information between the two end nodes via an intermediate relay node with the help of an IRS panel. Fig. 1 shows the IRS-assisted PNC system model we adopt in this work, where an IRS panel is placed to adjust the effective end nodes' uplink channels. The IRS has L reflectors, each has a reflection coefficient of $e^{j\theta_i}$, where the i th reflector adds a phase of θ_i to the incident signal before reflection. Let us assume that the two end nodes in the system are node A and node B , and they exchange information through the relay node, N_R .

We assume that the direct node-relay channels, v_A for node A and v_B for node B , are Rayleigh fading channels, and they are independent and identically distributed (i.i.d.). Strong node-IRS and IRS-relay links are typically available because

the IRS panel is always put in a place where it can have a line of sight (LoS) to the two end nodes and to the relay. Therefore, the IRS-relay channel vector, $\mathbf{g} \in \mathbb{C}^{L \times 1}$, can be modeled as Rician fading as

$$\mathbf{g} = \sqrt{\frac{pl(d_{I,N_R})K_{IN_R}}{K_{IN_R} + 1}} \mathbf{g}^{LoS} + \sqrt{\frac{pl(d_{I,N_R})}{K_{IN_R} + 1}} \mathbf{g}^{NLoS}, \quad (1)$$

where d_{I,N_R} is the IRS-relay distance, K_{IN_R} denotes the Rician factor of \mathbf{g} , \mathbf{g}^{LoS} and \mathbf{g}^{NLoS} are the line-of-sight (LoS) and non-LoS (NLoS) components, respectively. The LoS component is deterministic, however, the elements of \mathbf{g}^{NLoS} are i.i.d. complex normal, $\mathcal{CN}(0, 1)$, random variables. The channel vectors from the two end nodes to the IRS are \mathbf{h}_A and $\mathbf{h}_B \in \mathbb{C}^{L \times 1}$, and they can be expressed as

$$\mathbf{h}_m = \sqrt{\frac{pl(d_{m,I})K_{mI}}{K_{mI} + 1}} \mathbf{h}_m^{LoS} + \sqrt{\frac{pl(d_{m,I})}{K_{mI} + 1}} \mathbf{h}_m^{NLoS}, \quad m \in \{A, B\}, \quad (2)$$

where $d_{m,I}$ is the node-IRS distance, K_{mI} is the Rician factor of \mathbf{h}_m , \mathbf{h}_m^{LoS} and \mathbf{h}_m^{NLoS} are the LoS and NLoS components, respectively. All the channels in the system experience a path loss of pl , which is modeled as

$$pl(d) = \eta_0 \left(\frac{d}{d_0} \right)^{-\alpha}, \quad (3)$$

where α is the link path loss exponent, d is the transmitter-receiver radio frequency (RF) link distance, and η_0 is the path loss at the unit distance $d_0 = 1$ m.

Node A and node B exchange their messages through two steps: the first one is the multiple access (MA) step, and the second one is the broadcast (BC) step. During the MA step, nodes A and B simultaneously send their source messages to the relay. Hence, the relay receives a weighted sum of the two source messages, where the weights are the effective channel fading coefficients. Then, the relay, N_R , uses an appropriate mapping function to map the received weighted sum signal to a network-coded symbol. After that, the relay broadcasts the network-coded symbol to the two source nodes during the BC step so each of them can extract the other node's symbol from it. In the binary case, for example, the relay can map the received superimposed signal into the XOR of the two source binary data symbols. Assuming that the two transmitted source signals are x_A and x_B , the received superimposed signal at N_R can be written as

$$y_R = (\mathbf{h}_A^T \Theta \mathbf{g} + v_A) \sqrt{P_A} x_A + (\mathbf{h}_B^T \Theta \mathbf{g} + v_B) \sqrt{P_B} x_B + n, \quad (4)$$

where n is the complex Gaussian noise added at the relay having zero mean and variance of σ_n^2 , and P_A and P_B denote the transmit powers of node A and B , respectively. The diagonal matrix, Θ , contains the reflection coefficients of the IRS elements on its diagonal, i.e. $\Theta = \text{diag}(\mathbf{w})$, where $\mathbf{w} = [e^{j\theta_1}, e^{j\theta_2}, \dots, e^{j\theta_L}]^T$ and $\theta_i \in [0, 2\pi[$ denotes the phase shift of the i th reflector of the IRS. In the next section, we present an efficient algorithm to optimize the phase shifts of the IRS in a way that maximizes the received signals'

amplitudes at the relay while adhering to the constraint of cancelling the CPO between the two superimposed signals.

III. DESIGN OF THE IRS PHASE SHIFTS FOR PNC

In this section, we devise an algorithm to optimize the IRS reflection coefficients vector, \mathbf{w} , which maximizes the received signals' amplitude at the relay while satisfying the PNC design constraint. This constraint ensures canceling the CPO between the two received signals, i.e., the two signals having equal amplitudes and phases at the relay. Therefore, the optimization problem is given as

$$\max_{w_i} \quad |\mathbf{h}_A^T \Theta \mathbf{g} + v_A|^2 \quad (5a)$$

$$\text{s.t.} \quad C(\mathbf{w}) = \left| \sqrt{P_A} (\mathbf{h}_A^T \Theta \mathbf{g} + v_A) - \sqrt{P_B} (\mathbf{h}_B^T \Theta \mathbf{g} + v_B) \right| = 0 \quad (5b)$$

$$|w_i| = 1, \quad i = 1, 2, \dots, L, \quad (5c)$$

where $w_i = e^{j\theta_i}$ is the reflection coefficient of the i th reflector of the IRS.

The unit modulus constraints in (5c) form a smooth Riemannian manifold in \mathbb{C}^L called the complex circle manifold. Therefore, these constraints restrict the optimization vector, \mathbf{w} , and the solution of the problem (5) to be on the surface of the complex circle manifold, which can be expressed as

$$\mathcal{S}^L = \{\mathbf{w} = [w_1, \dots, w_L] \in \mathbb{C}^L : |w_1| = \dots = |w_L| = 1\}. \quad (6)$$

Therefore, in the following, we devise a manifold optimization-based technique to solve the IRS phase shifts problem in (5).

To handle the PNC alignment constraint in (5b), we adopt a standard method called the exact penalty method. Using this method, a weighted penalty can be added to the cost function using a penalty factor ρ to account for the constraint in (5b). If the constraint is violated during the optimization process, the weighted penalty term penalizes the objective function until the constraint is satisfied. Using the exact penalty method, our optimization problem becomes an unconstrained manifold optimization problem, which can be given as

$$\min_{w_i \in \mathcal{M}} \quad Q(\mathbf{w}) = -|\mathbf{h}_A^T \Theta \mathbf{g} + v_A|^2 + \rho C(\mathbf{w})^2, \quad (7)$$

where $\rho > 0$ is a penalty weight and \mathcal{M} is the Riemannian manifold.

By solving the optimization problem on the surface of the manifold \mathcal{M} , the unit modulus constraints in (5c) can be satisfied. The method is called *exact penalty* because only a bounded value of ρ is needed to satisfy the constraint in (5b). By transforming the original problem into an unconstrained manifold optimization problem, we can use gradient-based manifold optimization techniques to solve (7).

As in Euclidean spaces, there are two principal steps in the gradient-descent algorithm on Riemannian manifolds. The first step calculates a descent direction to move into, and the second step calculates the step size to be taken along that direction. After repeating these two steps over multiple iterations, the algorithm can converge to a locally optimal solution. The

descent direction on the manifold is called the *Riemannian gradient*, and it can be calculated by projecting the Euclidean gradient of the cost function at a given point on the manifold, \mathbf{w} , onto the tangent space at that point. The tangent space, $T_{\mathbf{w}}\mathcal{M}$, to a manifold, \mathcal{M} , at a point, \mathbf{w} , can be viewed as the space of possible velocities for a particle moving on the manifold through \mathbf{w} , and it can be expressed as

$$T_{\mathbf{w}}\mathcal{M} = \{\mathbf{v} \in \mathbb{C}^L : \Re(\mathbf{v} \odot \mathbf{w}^*) = \mathbf{0}_L\}, \quad (8)$$

where $\Re(\cdot)$ indicates the real-part of a complex vector, and \odot indicates the Hadamard entry-wise product of two vectors. Using a projection operator, the Riemannian gradient can then be calculated by projecting the Euclidean gradient onto the tangent space. The projection operator, $P_{T_{\mathbf{w}}\mathcal{M}}$, at point \mathbf{w} on \mathcal{M} is given by [25]

$$P_{T_{\mathbf{w}}\mathcal{M}}(\mathbf{v}) = \mathbf{v} - \Re(\mathbf{v} \odot \mathbf{w}^*) \odot \mathbf{w}. \quad (9)$$

Hence, the Riemannian gradient of the cost function, Q , in (7) at point \mathbf{w} on \mathcal{M} can be given as

$$\begin{aligned} \nabla_{\mathcal{M}} Q(\mathbf{w}) &= P_{T_{\mathbf{w}}\mathcal{M}}(\nabla Q(\mathbf{w})) \\ &= \nabla Q(\mathbf{w}) - \Re(\nabla Q(\mathbf{w}) \odot \mathbf{w}^*) \odot \mathbf{w}, \end{aligned} \quad (10)$$

where $\nabla Q(\mathbf{w})$ is the Euclidean gradient at the point \mathbf{w} .

Algorithm 1: Exact penalty method

```

1 Input: Initial point  $\mathbf{w}_0$ , initial penalty coefficient  $\rho_0$ ,
    $\gamma > 1$ ,  $\tau \geq 0$ , minimum step size  $d_{\min}$ .
2 for  $l = 0, 1, 2, \dots$  do
3   To attain  $\mathbf{w}_{l+1}$ , use any manifold optimization
   solver to solve
       
$$\min_{\mathbf{w} \in \mathcal{M}} Q(\mathbf{w}, \rho_l)$$

   with a starting point at  $\mathbf{w}_l$  and stopping indicator
   of
       
$$\|\text{grad } Q(\mathbf{w}, \rho_l)\| \leq \delta.$$

4   if  $\text{dist}(\mathbf{w}_l, \mathbf{w}_{l+1}) < d_{\min}$  and  $C(\mathbf{w}_{l+1}) > \tau$  then
5     | Return  $\mathbf{w}_{l+1}$ ;
6   end
7   if ( $k = 0$  or  $C(\mathbf{w}_{l+1}) \geq \tau$ ) then
8     |  $\rho_{l+1} = \gamma \rho_l$ 
9   else
10    |  $\rho_{l+1} = \rho_l$ ;
11  end
12 end

```

The steps of the exact penalty method which solves the unconstrained problem Q in (7) using the penalty coefficient, ρ , are illustrated in **Algorithm 1**. We use a common iterative approach, presented in [26], to update the value of ρ in each iteration till convergence. The value of ρ is set at a relatively low initial value; then we keep increasing it in each iteration if the PNC constraint (5b) is violated by being greater than a tolerance factor τ , as in lines 7 and 8 in **Algorithm 1**. In this case, ρ shall be increased to give more attention to satisfying

the constraint. The parameter ρ_l is increased by multiplying it with γ , a constant greater than one. The algorithm stops when the distance between the solutions of two successive iterations is below d_{\min} . The trust region solver [25] in the *Manopt* MATLAB tool [27] is used to solve the unconstrained manifold optimization problem (7), in line 3, during each iteration of the algorithm.

A. Complexity analysis

We then analyze the complexity of the proposed manifold optimization-based method presented in **Algorithm 1**. The complexity of **Algorithm 1** is determined by the complexity of solving the unconstrained manifold optimization problem in line 3 in each iteration. The complexity of solving the manifold optimization problem mainly depends on calculating the Euclidean gradient of the penalized cost function, Q , in (7) [28], which is given as $\mathcal{O}(L^2)$. Therefore, the overall complexity of **Algorithm 1** can be written as $\mathcal{O}(T_{Alg1}L^2)$, where T_{Alg1} is the number of iterations of **Algorithm 1**. Therefore, the proposed manifold optimization-based algorithm has a quadratic polynomial complexity with the number of IRS reflectors, L .

IV. CHANNEL CODED IRS-PNC WITH HIGH MODULATION ORDERS

In this section, higher modulation orders and channel coding are integrated into our IRS-assisted PNC system so it can be applied in real wireless systems. The IRS aligns the two effective channels of the two end nodes; this allows for designing simple PNC mapping functions at the relay with low decoding complexities. The received signal at the relay, in this case, can be written as

$$y_R = \Gamma x_A + \Gamma x_B + n, \quad (11)$$

where Γ is the overall effective channel after solving (5). We discuss an RA-channel coded PNC by designing the PNC mapping function at the relay when QPSK and 8-QAM modulation schemes are used at the two end nodes. The mapping function is appropriately designed to resolve any ambiguity in the decoded symbol at the relay. We further improve the performance of the RA-channel coded PNC by using weighted non-binary RA encoding over the Galois field at both end nodes.

In the WN-PNC, the binary data at both end nodes is mapped into the symbols of the GF. Then, the non-binary symbols are encoded using the weighted non-binary repeat accumulate (WNRA) codes discussed in [29] using the same non-binary weights, (w_1, w_2, w_3) , shown in Fig. 4. The non-binary data vectors are denoted by \mathbf{m}_A and \mathbf{m}_B , both of length L , and their corresponding codewords are denoted by \mathbf{c}_A and \mathbf{c}_B , both of length N , where the n th bit of a codeword is denoted by $c_{A,n}$ or $c_{B,n}$.

Fig. 4 shows the Tanner graph of the RA codes. In the encoding operation, the factor graph is traversed from left to right, given the values of the information nodes. The output of the GF addition, \oplus , is $c_{m,n} = c_{m,n-1} \oplus s_{m,n}$, where $m \in$

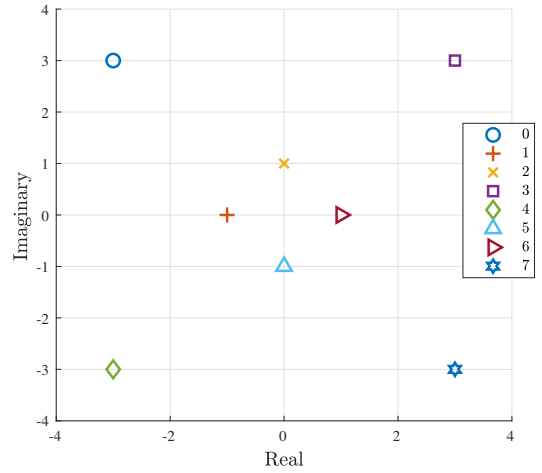


Figure 2: 8-QAM constellation

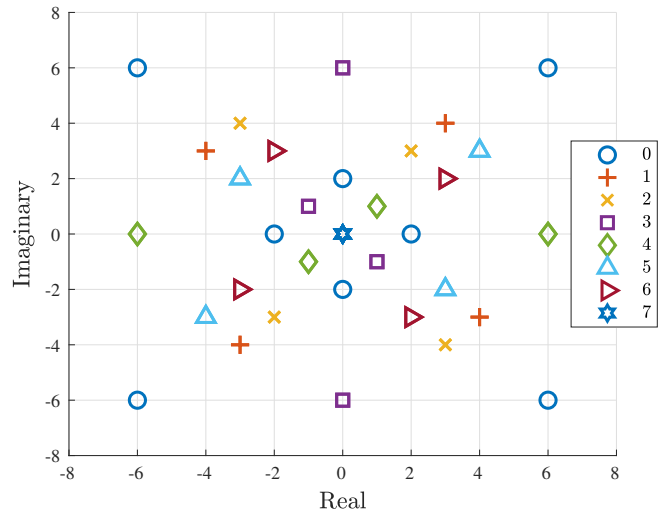


Figure 3: PNC mapping function of the 8-QAM modulation scheme

$\{A, B\}$. The value $s_{m,n}$ is the n th symbol after the interleaver of node m , and it equals the value of the k th input symbol to the interleaver, i.e., $s_{m,n} = u_{m,k}$. The interleaver in Fig. 4 determines how the index k is mapped to the index n . The RA encoders of the two end nodes must use the same interleaver.

The output non-binary coded symbols are then modulated by mapping them to complex constellation points x_A and x_B . The decoding of the WN-PNC is based on the detection of the GF-addition of the two codewords, $\mathbf{c}_A \oplus \mathbf{c}_B$, from the received superimposed signals at the relay. Therefore, the constellation mapping must be chosen to avoid ambiguity at the relay when detecting $\mathbf{c}_A \oplus \mathbf{c}_B$ from $x_A + x_B$. For the QPSK case, the constellation mapping that does not cause ambiguity can be $0 \rightarrow (-1, 1)$, $1 \rightarrow (1, 1)$, $2 \rightarrow (-1, -1)$ and $3 \rightarrow (1, -1)$. Therefore, the resultant unambiguous PNC mapping of $x_A + x_B$ to $c_{A,n} \oplus c_{B,n}$ at the relay is $\{(-2, 2), (2, 2), (-2, -2), (2, -2)\} \rightarrow 0$, $\{(0, 2), (0, -2)\} \rightarrow 1$, $\{(2, 0), (-2, 0)\} \rightarrow 2$, $(0, 0) \rightarrow 3$, where the GF addition is given in Table I. For the 8-QAM case, the constellation mapping at

-	0	1	2	3	4	5	6	7
0	0	1	2	3	4	5	6	7
1	1	0	3	2	5	4	7	6
2	2	3	0	1	6	7	4	5
3	3	2	1	0	7	6	5	4
4	4	5	6	7	0	1	2	3
5	5	4	7	6	1	0	3	2
6	6	7	4	5	2	3	0	1
7	7	6	5	4	3	2	1	0

Table I: GF(8) addition table

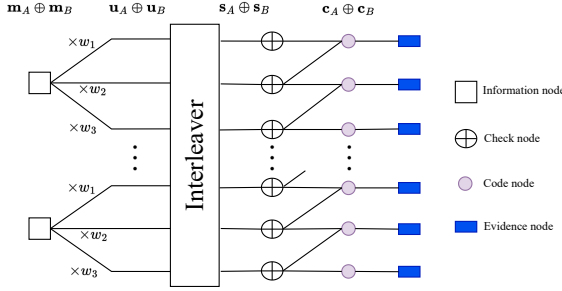


Figure 4: Factor graph for decoding network-coded data packets

the nodes that ensures no ambiguity is shown in Fig. 2, while the resultant unambiguous PNC mapping at the relay is shown in Fig. 3. Please note that the QPSK and 8-QAM constellations are scaled with a factor that ensures that the average power of the symbols of the constellations is unity.

The *distributive property* of the Galois field multiplication makes it feasible to decode the GF-addition of the two message vectors, $\mathbf{m}_A \oplus \mathbf{m}_B$, even after the multiplication with the weights. By using the same weights at both end nodes, we have

$$u_{A,k} \oplus u_{B,k} = w_i m_{A,l} \oplus w_i m_{B,l} = w_i (m_{A,l} \oplus m_{B,l}). \quad (12)$$

Hence, $\mathbf{m}_A \oplus \mathbf{m}_B$ can be decoded from $\mathbf{u}_A \oplus \mathbf{u}_B$ using belief propagation (BP) over the factor graph in Fig. 4. By calculating the probability mass function (PMF) of $c_{A,n} \oplus c_{B,n}$ given the n -th received symbol $y_{R,n}$, i.e. $P_{c_{A,n} \oplus c_{B,n}}(a) = \Pr(c_{A,n} \oplus c_{B,n} = a | y_{R,n}) \forall n$, the relay can obtain $\mathbf{m}_A \oplus \mathbf{m}_B$ using BP as follows.

The decoding of $\mathbf{m}_A \oplus \mathbf{m}_B$ from $c_{A,n} \oplus c_{B,n}$ is done by passing the input messages at the evidence nodes through the factor graph in Fig. 4. The input messages at the evidence nodes are the detected PMF vectors of $c_{A,n} \oplus c_{B,n}$. Then, these PMF vectors are iteratively passed between the code nodes and the information nodes in an iterative process called the BP. The edges that connect the information nodes with the check nodes carry the PMFs of $m_{A,l} \oplus m_{B,l}$ before multiplication by the weights. However, the segments that connect the code nodes with the check nodes or the evidence nodes carry the PMFs of $c_{A,n} \oplus c_{B,n}$.

Initialization: The PMFs on all the edges are initialized as a length-4 vector whose elements are $1/4$ in the GF(4) case, and a length-8 vector whose elements are $1/8$ in the GF(8) case.

Input of the Evidence Nodes: The PMF vectors of the GF sum of the two code words symbols, $c_{A,n} \oplus c_{B,n}$ are the

input messages to the BP algorithm. These input messages are passed from the evidence nodes. Let's indicate the input PMF vector at the n th evidence node by \mathbf{p}_n . Given $y_{R,n}$, the probability that $c_{A,n} \oplus c_{B,n} = i$ which is the $(i+1)$ th element of \mathbf{p}_n can be calculated as

$$p_{n,i} = \frac{1}{\beta} \sum_{x \in \mathcal{X}_i} p_x \exp \left\{ \frac{-|y_{R,n} - \Gamma x|^2}{2\sigma^2} \right\}, \quad (13)$$

where p_x is the prior probability of the point x , \mathcal{X}_i is the set of points that map to the symbol i in the GF, and β is a normalization factor which ensures that $\frac{1}{\beta} \sum_{i=0}^I p_{n,i} = 1$, and I is 3 or 7 for the GF(4) and GF(8) cases, respectively.

Message Updating at the Variable Nodes: The information nodes and the code nodes are called variable nodes. If the considered RA encoder has a repetition factor of 3, then the variable nodes in Fig. 4 should be attached to three distinct edges. Given that the two input messages on two connected edges of a variable node are \mathbf{p} and \mathbf{q} , the output updated message on the third edge is given by $VAR(\mathbf{p}, \mathbf{q})$. By employing a similar probabilistic analysis as in [30], the output message vector of the variable node can be given as

$$VAR(\mathbf{p}, \mathbf{q}) = \frac{1}{\zeta} (p_0 q_0, p_1 q_1, \dots, p_I q_I), \quad (14)$$

where ζ is a normalization factor which ensures that $\frac{1}{\zeta} \sum_{i=0}^I p_i q_i = 1$.

Message Updating for the Check Nodes: As shown in Fig. 4, the check nodes are connected to three edges. The output message vector of a check node is given by $CHK(\mathbf{p}, \mathbf{q})$, where \mathbf{p} and \mathbf{q} are the input message vectors coming from the remaining two connected edges. The output message of the check node during the BP algorithm is calculated as follows. For example, in the following, let us consider the GF(4) case. Assuming that $S = s_{A,n} \oplus s_{B,n}$, $\bar{C} = c_{A,n-1} \oplus c_{B,n-1}$, and $C = c_{A,n} \oplus c_{B,n}$, the probability that the symbol C is equal to 0 given the two input messages \mathbf{p} and \mathbf{q} , knowing that $C = S \oplus \bar{C}$ and given the addition table in Table I, can be computed as

$$\begin{aligned} & \Pr(C = 0 | \bar{C} \sim \mathbf{p}, S \sim \mathbf{q}) \\ &= \sum_{i=0}^3 \Pr(\bar{C} = i) \Pr(C = 0 | \bar{C} = i, S \sim \mathbf{q}) \\ &= \Pr(\bar{C} = 0 | \mathbf{p}) \Pr(S = 0 | \mathbf{q}) + \Pr(\bar{C} = 1 | \mathbf{p}) \Pr(S = 1 | \mathbf{q}) \\ &+ \Pr(\bar{C} = 2 | \mathbf{p}) \Pr(S = 2 | \mathbf{q}) + \Pr(\bar{C} = 3 | \mathbf{p}) \Pr(S = 3 | \mathbf{q}) \\ &= p_0 q_0 + p_1 q_1 + p_2 q_2 + p_3 q_3, \end{aligned} \quad (15)$$

where $S \sim \mathbf{q}$ means that the discrete random variable S has a PMF vector of \mathbf{q} . Similarly, the probabilities of C taking other values can be calculated to produce the check node's output PMF vector.

V. SIMULATION RESULTS

In this section, we evaluate the performance of the proposed IRS-assisted PNC system and show the effectiveness of the proposed manifold optimization-based algorithm to optimize the IRS reflectors. Moreover, the performance of the WN-PNC discussed in Sec. IV is also evaluated and compared against the

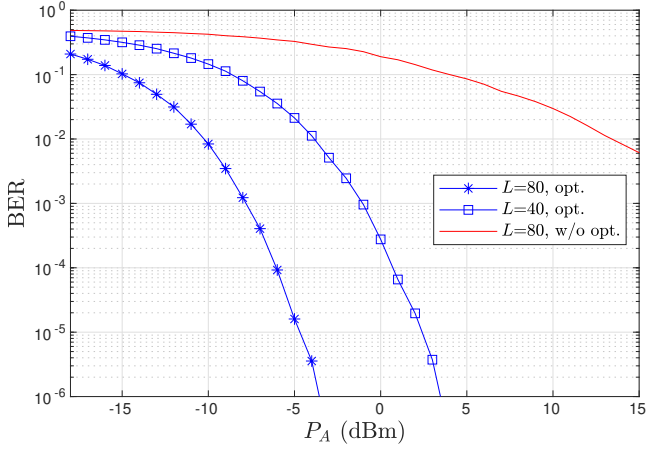


Figure 5: BER performance of the IRS-assisted PNC scenario

non-binary PNC without weights as well as the conventional binary encoding cases. The performance of the WN-PNC is provided for both QPSK and 8-QAM modulation schemes. In all figures, we plot the bit error rate (BER) of the detected network-coded signal at the relay.

The simulation parameters are provided in this paragraph, following the model in [6]. The path loss at the reference distance in (3) is $\eta_0 = 10^{-3}$. The node-relay links' path loss exponent, α , is set to 3.5, whereas the path loss exponent of the node-IRS and IRS-relay links is set to 2.2. The Rician factors in (1) and (2) are set as $K_{IN_R} = K_{mI} = 2.2$. The noise power σ_n^2 is assumed as -114 dBm. The node-IRS distances are $d_{A,I} = 60$ and $d_{B,I} = 60$, whereas the IRS-relay distance is $d_{I,N_R} = 30$. We plot all the BER curves against P_A , while we assume that $P_B = P_A$.

In Fig. 5, we present the BER performance of the IRS-assisted PNC scenario when optimizing the IRS phase shifts using the proposed manifold optimization-based approach in **Algorithm 1**. In this figure, we evaluate the performance using the simple binary phase shift keying (BPSK) modulation scheme, where the data is drawn from binary symbols over GF(2). Maximum likelihood (ML) detection is used to detect the network-coded signal at the relay, which is the XOR between the two binary source symbols. The performance of the optimized IRS-phases system is compared against IRS-assisted PNC system without manifold-based optimization, i.e., when picking up any random feasible solution that satisfies the PNC constraint in (5). Any feasible solution that satisfies (5) will cancel the CPO between the two received superimposed signals at the relay and align them in the PNC fashion, i.e., having equal amplitudes and phases. However, this random feasible solution does not necessarily maximize the received signals' amplitude, $\Gamma_{opt} = \sqrt{P_A}(\mathbf{h}_A^T \Theta_{opt} \mathbf{g} + v_A)$, at the relay. Therefore, Fig. 5 shows that the system's performance with optimization outperforms the performance without using the proposed manifold optimization technique. The graph also shows, and as expected, that as the number of IRS reflectors, L , increases, the BER of the IRS assisted PNC system decreases.

In the next two figures, we use the following simulation

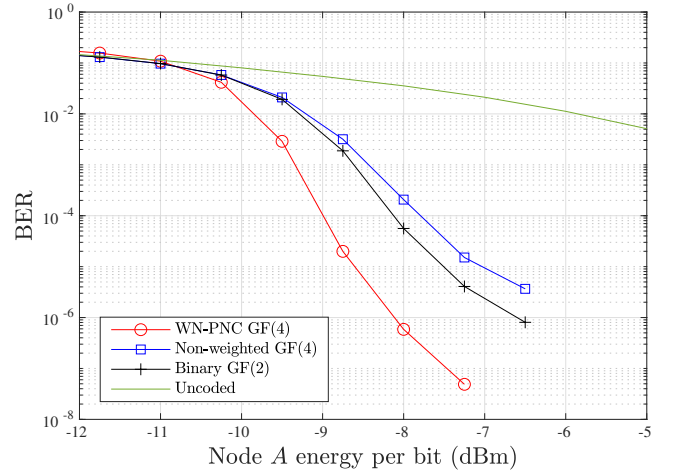


Figure 6: Performance comparison of WN-PNC over GF(4) against conventional coding schemes using QPSK

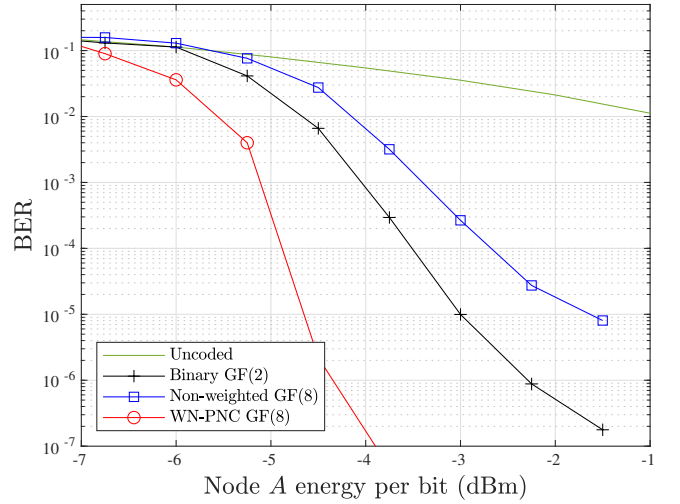


Figure 7: Performance comparison of WN-PNC over GF(8) against conventional coding schemes using 8-QAM

parameters; the length of the uncoded binary data vector is set to 2048, and the repetition factor of the channel encoder is 3. The error performance at every point is calculated by taking the average over 10000 data packets that every node generates. The relay can then decode a network-coded data vector from the received superimposed codewords. The number of considered iterations of the BP decoding algorithm is set to 20. The number of IRS reflectors is $L = 40$. We use the weights discussed in [29], where (w_1, w_2, w_3) , are $(1, \alpha, \alpha^2)$ for both GF(4) and GF(8) cases. The value of α is any value over the GF except 0 and 1.

Fig. 6 and Fig. 7 show the BER performance of the channel coded WN-PNC system using QPSK and 8-QAM modulation schemes, respectively. In Fig. 6, the binary data are mapped to symbols in GF(4), encoded over GF(4) then modulated using QPSK. Whereas, in Fig. 7, the binary data are mapped to symbols in GF(8), encoded over GF(8) then modulated using 8-QAM constellation provided in Fig. 2. In both figures, we notice that the GF(4) or GF(8) encoding without weights

provides worse performance than the binary encoding scheme. In the binary encoding, the data are encoded over GF(2) then the output binary bits are modulated normally to QPSK or 8-QAM. However, the figures show that by using the weights, the WN-PNC coding scheme outperforms both the binary and the non-weighted coding schemes. This enhances the performance of the channel coded PNC system. The three channel-coded PNC schemes are also compared against the uncoded PNC case using the same modulation scheme and transmitted energy per bit to highlight the effect of channel coding on the system's performance.

VI. CONCLUSIONS

In this work, we showed how the IRS could enhance the performance of the IRS-assisted PNC system in a TWRC. The IRS can completely eliminate the CPO problem between the two end nodes. Moreover, our simulation results show that optimizing the IRS phase shifts using the proposed manifold-based optimization algorithm can significantly enhance the system's BER performance. Finally, although the results show that the encoding schemes over GF(4) and GF(8) result in worse BER performance compared to the binary encoding over GF(2), we showed, using simulations, that the proposed WN-PNC scheme can enhance the system BER performance over the binary encoding scheme by using some proper weights.

ACKNOWLEDGEMENT

This work was supported by the European Union's Horizon 2020 Research and Innovation Program through the Marie Skłodowska-Curie under grant agreement number 812991.

REFERENCES

- [1] S. C. Liew, S. Zhang, and L. Lu, "Physical-layer network coding: Tutorial, survey, and beyond," *Physical Commun.*, vol. 6, pp. 4–42, 2013, network Coding and its Applications to Wireless Communications.
- [2] E. Basar, M. Di Renzo, J. De Rosny, M. Debbah, M.-S. Alouini, and R. Zhang, "Wireless communications through reconfigurable intelligent surfaces," *IEEE Access*, vol. 7, pp. 116 753–116 773, 2019.
- [3] M. Di Renzo, M. Debbah, D.-T. Phan-Huy, A. Zappone, M.-S. Alouini, C. Yuen, V. Sciancalepore, G. C. Alexandropoulos, J. Hoydis, H. Gacanin, J. de Rosny, A. Bounceur, G. Lerosey, and M. Fink, "Smart radio environments empowered by reconfigurable ai meta-surfaces: an idea whose time has come," *EURASIP J. Wireless Commun. Netw.*, 2019.
- [4] M. A. ElMossallamy, H. Zhang, L. Song, K. G. Seddik, Z. Han, and G. Y. Li, "Reconfigurable intelligent surfaces for wireless communications: Principles, challenges, and opportunities," *IEEE Trans. Cognitive Commun. Netw.*, vol. 6, no. 3, pp. 990–1002, 2020.
- [5] Q. Wu, S. Zhang, B. Zheng, C. You, and R. Zhang, "Intelligent reflecting surface-aided wireless communications: A tutorial," *IEEE Trans. Commun.*, vol. 69, no. 5, pp. 3313–3351, 2021.
- [6] Q. Wu and R. Zhang, "Intelligent reflecting surface enhanced wireless network via joint active and passive beamforming," *IEEE Trans. Wireless Commun.*, vol. 18, no. 11, pp. 5394–5409, 2019.
- [7] C. Huang, A. Zappone, G. C. Alexandropoulos, M. Debbah, and C. Yuen, "Reconfigurable intelligent surfaces for energy efficiency in wireless communication," *IEEE Trans. Wireless Commun.*, vol. 18, no. 8, pp. 4157–4170, 2019.
- [8] C. Huang, R. Mo, and C. Yuen, "Reconfigurable intelligent surface assisted multiuser miso systems exploiting deep reinforcement learning," *IEEE J. Sel. Areas Commun.*, vol. 38, no. 8, pp. 1839–1850, 2020.
- [9] M. A. ElMossallamy, H. Zhang, R. Sultan, K. G. Seddik, L. Song, G. Y. Li, and Z. Han, "On spatial multiplexing using reconfigurable intelligent surfaces," *IEEE Wireless Commun. Lett.*, vol. 10, no. 2, pp. 226–230, 2021.
- [10] M. Zeng, X. Li, G. Li, W. Hao, and O. A. Dobre, "Sum rate maximization for ired-assisted uplink noma," *IEEE Commun. Lett.*, vol. 25, no. 1, pp. 234–238, 2021.
- [11] X. Mu, Y. Liu, L. Guo, J. Lin, and N. Al-Dhahir, "Exploiting intelligent reflecting surfaces in noma networks: Joint beamforming optimization," *IEEE Trans. Wireless Commun.*, vol. 19, no. 10, pp. 6884–6898, 2020.
- [12] G. Yang, X. Xu, and Y.-C. Liang, "Intelligent reflecting surface assisted non-orthogonal multiple access," in *2020 IEEE Wireless Commun. Netw. Conf. (WCNC)*, 2020, pp. 1–6.
- [13] C. Pan, H. Ren, K. Wang, M. Elkashlan, A. Nallanathan, J. Wang, and L. Hanzo, "Intelligent reflecting surface aided mimo broadcasting for simultaneous wireless information and power transfer," *IEEE J. Sel. Areas Commun.*, vol. 38, no. 8, pp. 1719–1734, 2020.
- [14] Q. Wu, X. Guan, and R. Zhang, "Intelligent reflecting surface-aided wireless energy and information transmission: An overview," *Proceedings of the IEEE*, vol. 110, no. 1, pp. 150–170, 2022.
- [15] M. Al-Jarrah, E. Alsusa, A. Al-Dweik, and D. K. C. So, "Capacity analysis of ired-based uav communications with imperfect phase compensation," *IEEE Wireless Commun. Lett.*, vol. 10, no. 7, pp. 1479–1483, 2021.
- [16] X. Zhou, S. Yan, Q. Wu, F. Shu, and D. W. K. Ng, "Intelligent reflecting surface (irs)-aided covert wireless communications with delay constraint," *IEEE Trans. Wireless Commun.*, vol. 21, no. 1, pp. 532–547, 2022.
- [17] L. Lu and S. C. Liew, "Asynchronous physical-layer network coding," *IEEE Trans. Wireless Commun.*, vol. 11, no. 2, pp. 819–831, 2012.
- [18] L. Yang, T. Yang, J. Yuan, and J. An, "Achieving the near-capacity of two-way relay channels with modulation-coded physical-layer network coding," *IEEE Trans. Wireless Commun.*, vol. 14, no. 9, 2015.
- [19] H. Zhang, L. Zheng, and L. Cai, "Design and analysis of heterogeneous physical layer network coding," *IEEE Trans. Wireless Commun.*, vol. 15, no. 4, 2016.
- [20] H. Zhang and L. Cai, "Design of channel coded heterogeneous modulation physical layer network coding," *IEEE Trans. Veh. Technol.*, vol. 67, no. 3, 2018.
- [21] S. Shukla, V. T. Muralidharan, and B. S. Rajan, "Wireless network-coded accumulate–compute-and-forward two-way relaying," *IEEE Trans. Veh. Technol.*, vol. 65, no. 3, pp. 1367–1381, 2016.
- [22] L. Guo, Z. Ning, Q. Song, Y. Cui, and Z. Chen, "Toward efficient 5G transmission: SER performance analysis for asynchronous physical-layer network coding," *IEEE Access*, vol. 4, pp. 5083–5097, 2016.
- [23] Z. Wang and S. C. Liew, "Coherent detection for short-packet physical-layer network coding with binary FSK modulation," *IEEE Trans. Wireless Commun.*, vol. 19, no. 1, pp. 279–292, 2020.
- [24] M. AlaaEldin, E. Alsusa, and K. G. Seddik, "Irs-assisted physical layer network coding over two-way relay fading channels," *IEEE Trans. Veh. Technol.*, vol. 71, no. 8, pp. 8424–8440, 2022.
- [25] P.-A. Absil, R. Mahony, and R. Sepulchre, *Optimization Algorithms on Matrix Manifolds*. Princeton, NJ: Princeton University Press, 2008.
- [26] C. Liu and N. Boumal, "Simple algorithms for optimization on riemannian manifolds with constraints," *Appl Math Optim.*, vol. 82, no. 3, pp. 949–981, 2020.
- [27] N. Boumal, B. Mishra, P.-A. Absil, and R. Sepulchre, "Manopt, a MATLAB toolbox for optimization on manifolds," *J. Machine Learning Research*, vol. 15, no. 42, pp. 1455–1459, 2014. [Online]. Available: <https://www.manopt.org>
- [28] X. Yu, D. Xu, and R. Schober, "MISO wireless communication systems via intelligent reflecting surfaces : (invited paper)," in *2019 IEEE/CIC Int. Conf. Commun. in China (ICCC)*, 2019, pp. 735–740.
- [29] K. Yang, "Weighted non-binary repeat-accumulate codes," *IEEE Trans. Inf. Theory*, vol. 50, no. 3, pp. 527–531, 2004.
- [30] S. Zhang and S.-C. Liew, "Channel coding and decoding in a relay system operated with physical-layer network coding," *IEEE J. Sel. Areas Commun.*, vol. 27, no. 5, pp. 788–796, 2009.